



## OPEN ACCESS

## EDITED BY

Longxiang Zhu,  
Chongqing University, China

## REVIEWED BY

Di Wang,  
China Nuclear Power Technology  
Research Institute, China  
Hui Cheng,  
Harbin Engineering University, China

## \*CORRESPONDENCE

Xing-Kang Su,  
✉ [suxk@lzu.edu.cn](mailto:suxk@lzu.edu.cn)

RECEIVED 15 July 2023

ACCEPTED 05 September 2023

PUBLISHED 22 September 2023

## CITATION

Chen Q-J, Qiu J, Zhang J-B, Guo Y-F,  
Su X-K, Gu L and Liu J-T (2023), Sub-  
channel analysis for LBE cooled fuel  
assembly with grid type spacers of China  
initiative accelerator driven system.  
*Front. Energy Res.* 11:1259254.  
doi: 10.3389/fenrg.2023.1259254

## COPYRIGHT

© 2023 Chen, Qiu, Zhang, Guo, Su, Gu  
and Liu. This is an open-access article  
distributed under the terms of the  
[Creative Commons Attribution License  
\(CC BY\)](https://creativecommons.org/licenses/by/4.0/). The use, distribution or  
reproduction in other forums is  
permitted, provided the original author(s)  
and the copyright owner(s) are credited  
and that the original publication in this  
journal is cited, in accordance with  
accepted academic practice. No use,  
distribution or reproduction is permitted  
which does not comply with these terms.

# Sub-channel analysis for LBE cooled fuel assembly with grid type spacers of China initiative accelerator driven system

Qi-Jian Chen<sup>1</sup>, Jing Qiu<sup>1</sup>, Jin-Biao Zhang<sup>1</sup>, Yue-Feng Guo<sup>1</sup>,  
Xing-Kang Su<sup>1\*</sup>, Long Gu<sup>1,2,3</sup> and Jia-Tai Liu<sup>4</sup>

<sup>1</sup>School of Nuclear Science and Technology, Lanzhou University, Lanzhou, China, <sup>2</sup>Institute of Modern Physics, Chinese Academy of Sciences, Lanzhou, China, <sup>3</sup>School of Nuclear Science and Technology, University of Chinese Academy of Sciences, Beijing, China, <sup>4</sup>China Nuclear Power Engineering Co. LTD., Beijing, China

The present study focuses on the thermal hydraulic characteristics of fuel assemblies in the China Initiative Accelerator Driven subcritical System (CiADS), which utilizes grid-type spacers to support lead bismuth eutectic (LBE) cooled fast reactors. While the structural design and mechanical analysis of CiADS triangular fuel assemblies with grid-type spacers have been preliminarily investigated, there is a pressing need to study the thermal hydraulic behavior of liquid LBE within these fuel assemblies. This analysis is crucial for assessing the safety and economy of the CiADS subcritical reactor. The sub-channel analysis code, based on the lumped parameter method, plays a vital role in rapidly evaluating the safety features of LBE-cooled fast reactor fuel assemblies. To comprehensively evaluate the thermal hydraulic performance of fuel assemblies with grid-type spacers in the CiADS LBE cooling system, the flow pressure drop model, turbulent mixing model, and convective heat transfer model for the fuel assembly structure with grid-type spacers were incorporated into the existing CiADS sub-channel analysis code. This enhanced code has been successfully employed in the thermal hydraulic analysis of fuel assemblies utilizing wire-type spacers in the CiADS system. To verify the validity and accuracy of the modified CiADS sub-channel analysis code in calculating triangular fuel assemblies with grid-type spacers, the code was first utilized to replicate a 19-rods flow heat transfer experiment with grid-type spacers cooling liquid LBE. A comparison between the simulation and experimental results confirms that the CiADS sub-channel analysis code can predict the coolant temperature and fuel rod surface temperature in fuel assemblies with grid-type spacers. Subsequently, the structure and thermal hydraulic design of the latest CiADS fuel assembly with grid-type spacers were reviewed. Finally, taking into account the aforementioned enhancements to the CiADS sub-channel analysis code, a comprehensive thermo-hydraulic calculation of the CiADS fuel assembly with grid-type spacers was conducted. The results demonstrate that the coolant outlet temperature, maximum cladding temperature, and maximum fuel pellet temperature all fall within the design parameters of CiADS. Furthermore, the impact of the number of rods in different rod bundles (91, 61, 37, and 7 rods) on thermal hydraulic performance was analyzed. The findings indicate that, while ensuring calculation accuracy and efficiency, the results obtained from the 37-rod bundle can effectively reflect the thermal hydraulic behavior of the reactor core.

## KEYWORDS

CiADS, lead bismuth eutectic, grid spacers, sub-channel analysis, thermal-hydraulic

## 1 Introduction

Liquid lead and lead bismuth eutectic (LBE) are emerging as promising coolants for next-generation advanced nuclear energy systems, primarily due to their superior thermal-hydraulic properties, increased inertness, and optimal neutron characteristics (Abram and Ion, 2008). Both the China Initiative Accelerator Driven Subcritical System (CiADS) (Gu and Su, 2021) and the Multi-purpose Hybrid Research Reactor for High-tech Applications (MYRRHA) (Abderrahim et al., 2012) have identified liquid LBE as the preferred coolant in their subcritical reactors. The CiADS project, however, faced technical and engineering challenges. This led to the formulation of two distinct fuel assembly designs: wire-type spacers and grid-type spacers. The aim was to thoroughly assess and integrate these designs into the CiADS framework. Initial research was directed toward the design and thermal-hydraulic engineering of LBE-cooled fuel assemblies using wire-type spacers (Peng et al., 2017). Recent developments in the structural design of the CiADS triangular fuel assembly with wire-type spacers were highlighted by Yu et al. (2021). Furthermore, Fan et al. (2020) embarked on flow experiments with wire-wrapped 19-rod bundles tailored for CiADS. Using the Reynolds analogy and visualization methods, they derived the flow pressure drop and cross-sectional pressure drop profiles for the wire-type spacer's fuel assembly. On the computational side, Liu et al. (2022) fine-tuned a sub-channel analysis code for simulating thermo-hydraulics of wire-type spacer fuel assemblies cooled by liquid LBE. Leveraging this code, they analyzed the thermo-hydraulic characteristics of a comprehensive 61-rod wire-type spacers fuel assembly.

Wire-type spacers play a pivotal role in preserving the ideal spacing of fuel rods, curtailing mechanical vibrations, bolstering turbulent mixing among sub-channels, and avoiding temperature peaks. However, these spacers increase flow resistance. Conversely, grid-type spacers, with their compact volume, permit a more substantial core allocation for fuel, thereby amplifying the breeding ratio and diminishing the doubling time. Furthermore, the built-in flow channels in the fuel assembly are straightforward, reducing flow resistance and the risk of obstructions from LBE corrosion impurities. Preliminary research at CiADS has addressed the structural design and the hydrostatic and dynamic attributes of the triangular fuel assembly with grid-type spacers (Sheng, 2022). It is imperative now to delve deeper into the thermal hydraulics of liquid LBE within this structure, ensuring alignment with CiADS thermal design norms. The sub-channel analysis method strikes a balance between the detailed three-dimensional computational fluid dynamics approach and the simplified one-dimensional system safety assessment, offering an efficient, cost-effective, and swift assessment of LBE's thermal hydraulics in the fuel assembly. Several renowned codes cater to the thermal hydraulic evaluation of liquid metal-cooled fast reactors: 1) COBRA-WC (George et al., 1980), which can simulate multiple fuel assemblies at the same time as well as several operating conditions including forced and natural cycles. 2) MATRA-LMR (Kim et al., 2002), which uses the distributed resistance model and improves the sodium properties, heat transfer relations and pressure drop relations. 3) ATHAS-LMR (Chen, 2012), which deduces a three-dimensional drag model instead of the lumped parameter method by theory, and finally calculates the experimental results of the flow blockage accident

in the liquid metal fast neutron breeder reactor. The results show that the calculated results are in good agreement with the experimental results. 4) SACOS-PB (Wang et al., 2013a), which is concluded that the hexagonal fuel assembly is the best choice for the LBE fast reactor by analyzing the temperature distribution of the fuel assembly and diverse component types. Wu et al. (2021) improved SACOS-PB, and Wang et al. (2021) utilized it for flow blockage incident analysis. 5) ANTEO+ (Lodi et al., 2016a), which can be used to calculate liquid metal cooled fast reactors, including sodium, lead, LBE, and is suitable for a variety of geometric structures such as bare-rod, grid-type spacers, and wire-type spacers. 6) KMC-sub (Li et al., 2017), which adds the relation applicable to liquid LBE and is used to calculate the steady-state condition of SNCLFR-100. (7)

Conducting heat transfer experiments using LBE is challenging due to its corrosive and opaque nature (Schroer et al., 2012). For the purpose of generating experimental data and validating sub-channel analysis codes specifically designed for LBE-cooled fuel assemblies with spacer grids, several notable experiments have been undertaken: 1) Pacio et al. (2014) constructed the THEADES loop at the Karlsruhe Liquid Metals Laboratory (KALLA) with reference to the geometry of MYRRHA. They used 19 rods with grid-type spacers and conducted heat transfer experiments under steady-state and forced convection conditions. 2) Di Piazza et al. (2016) also carried out a heat transfer experiment with 19 rods using wire-type spacers in the NACIE-UP circuit for the MYRRHA reactor. Unlike the experiments by Pacio et al., the NACIE-UP loop experiments adopted steady-state, adiabatic, and natural cycles, and placed more focus on the heat transfer phenomenon of liquid LBE at a low flow rate ( $Re = 1000-10000$ ). 3) Lyu et al. (2016) carried out heat transfer experiments of 61 rods bundle wire-wrapped fuel assemblies on the KYLIN-II lead reactor comprehensive experimental circuit, in which the experimental sections included a 350 mm inlet flow section, a 800 mm heating section and a 132 mm outlet flow section, in order to eliminate the effect of inlet flow instability and outlet effect on the heating section. In these experiments, Pacio et al. carried out a detailed study on the heat transfer process of high-temperature liquid LBE in 19 rods bundle with grid-type spacers, and obtained multiple groups of coolant temperatures and heating rod temperatures, which were widely applied to the validation of sub-channel analysis code for LBE cooling.

Since most of the sub-channel analysis code are closed-source, for the sake of studying the thermal hydraulic characteristics of CiADS LBE cooling fuel assemblies with grid-type spacers, this study is based on the optimization of the sub-channel analysis code for LBE cooling winding fuel assemblies with grid-type spacers by Liu et al. (2022). By incorporating flow pressure drop, convective heat transfer, and turbulent mixing models suitable for the fuel assembly with grid-type spacers cooled by lead and bismuth, the code's development aims to analyze the thermal hydraulics of the CiADS lead and bismuth-cooled fuel assembly with grid-type spacers. The validity and reliability of the sub-channel analysis code developed in this study were verified by using the available information of 19 rods with grid-type spacers heat transfer experiments cooled by lead and bismuth. Then, based on the current version of the sub-channel analysis code, the thermal hydraulic behavior of coolant temperature, cladding temperature and fuel rod temperature distribution for a single CiADS full-size fuel assembly with grid-type spacers was investigated. Previously, the latest structural design and thermal hydraulic of the current

CiADS LBE cooled fuel assemblies with grid-type spacers were reviewed. Finally, the influence of different rod numbers on the internal temperature distribution characteristics of the fuel assembly is analyzed. By incorporating the flow pressure drop model, convective heat transfer model, and turbulent mixing model suitable for the fuel assembly with grid-type spacers cooled by lead and bismuth, the code's development aims to analyze the thermal hydraulics of the CiADS lead and bismuth cooled fuel assembly with grid-type spacers. The validity and reliability of the sub-channel analysis code developed in this study were verified using the available data from heat transfer experiments involving 19 rods with grid-type spacers cooled by lead and bismuth. Subsequently, based on the current version of the sub-channel analysis code, the thermal hydraulic behavior of coolant temperature, cladding temperature, and fuel rod temperature distribution for a single full-size CiADS fuel assembly with grid-type spacers was investigated. Furthermore, the latest structural design and thermal hydraulics of the current CiADS LBE-cooled fuel assemblies with grid-type spacers were reviewed. Finally, the influence of different rod numbers on the internal temperature distribution characteristics of the fuel assembly is analyzed.

## 2 Sub-channel code for LBRF

The main purpose of the sub-channel analysis code is to accurately calculate and analyze the thermal hydraulic behavior of coolant and fuel rods in fuel assemblies. Due to the significantly higher boiling point of liquid lead compared to the operating temperature within the reactor, the coolant can be treated as a single-phase flow without boiling. The code utilizes discrete mass, axial momentum, transverse momentum, and energy conservation equations to calculate the mass flow rate and temperature distribution of coolant in different sub-channels. The conservation equations for incompressible fluids are solved using the finite difference method, which ensures the conservation of the total mass entering and leaving a control volume. The thermal hydraulic parameters are then calculated using the conservation equations for mass, energy, and momentum (Liu et al., 2022).

Mass Conservation Equation:

$$A \frac{\partial \rho}{\partial t} + \frac{\partial m}{\partial z} + \sum_{k \in i} e_{ik} w = 0 \quad (1)$$

where  $A$  is the axial flow area;  $\rho$  is the coolant density;  $t$  is the time;  $m$  is the axial mass flow;  $\Delta z$  is the axial control body height;  $e_{ik}$  is the symbolic function;  $w$  is the unit length transverse mass flow. Each term of the equation is the change of mass with time, the change of axial mass flow with space, and the total transverse mass flow in and out of the gap.

Energy Conservation Equation:

$$A \frac{\partial \rho h}{\partial t} + \frac{\partial m h}{\partial z} + \sum_{k \in i} e_{ik} w h^* = \sum_{k \in i} P_W \phi_{ir} q + \sum_{k \in i} C_Q \phi_{in} q' - \sum_{k \in i} w' \Delta h - \sum_{k \in i} C_k s \Delta T \quad (2)$$

where  $h$  is the enthalpy of the fluid;  $P_W$  is the heating perimeter of the fuel rod  $r$  facing the subchannel  $i$ ;  $\phi_{ir}$  is the share of fuel rod  $r$  facing channel  $i$ ;  $q$  is the linear power density of the fuel rod;  $C_Q$  is

the heat production share of the coolant;  $\phi_{in}$  is the contact share between the fuel rod and the channel;  $q'$  is the line power density of fuel rod incoming the coolant;  $\Delta h$  is the enthalpy difference between adjacent channels;  $C_k$  is the transverse heat transfer coefficient and  $\Delta T$  is the temperature difference between adjacent channels.

Axial Momentum Conservation Equation:

$$\frac{\partial m}{\partial t} + \frac{\partial m U}{\partial z} + \sum_{k \in i} e_{ik} w U = -A \frac{\partial p}{\partial z} - \rho g A \cos \theta - \frac{1}{2} \rho U^2 A \left( \frac{f}{D} + \frac{K}{\Delta z} \right) - f_T \sum_{k \in i} e_{ik} w' U \quad (3)$$

where  $U$  is the axial flow rate;  $P$  is the pressure;  $g$  is the acceleration of gravity;  $\theta$  is the angle between the coolant channel and the vertical direction;  $f$  is the friction coefficient;  $D$  is the diameter of fuel rod;  $K$  is the form resistance coefficient;  $f_T$  is the turbulent momentum exchange coefficient and  $w'$  is the turbulent mixing flow per unit length.

Transverse Momentum Conservation Equation:

$$\frac{\partial w}{\partial t} + \frac{\partial w U}{\partial z} = \frac{s}{l} \Delta p - K_G \frac{s}{l} \frac{w |w|}{2 \rho s^2} \quad (4)$$

where  $l$  is the centroid distance between sub-channel  $i$  and sub-channel  $k$ .  $K_G$  is the lateral resistance coefficient. The items on Eq. 4 left side are the variation of transverse flow rate with time and the variation of transverse flow flux with space. The items on Eq. 4 right side are the transverse pressure difference term and clearance resistance term.

This chapter introduces the friction pressure drop model, convective heat transfer model, and turbulent mixing model that have been integrated into the code. Furthermore, the correlations for physical properties and fundamental numerical analysis models continue to rely on the sub-channel code COBRA-LFR developed by Liu et al. (2022).

### 2.1 Friction resistance model

During the calculation of sub-channel pressure drop, the overall pressure drop is divided into two components: the pressure drop across the rod bundle and the resistance pressure drop across the grid-type spacers. Attaining appropriate values for the friction coefficient and spacer loss coefficient is crucial to ensuring the accuracy of the friction pressure drop calculation. The Darcy-Weisbach formula, represented by Eq. 5, can be employed to compute the pressure drop, specifically for the rod bundle pressure drop.

$$\Delta p = f \frac{L}{De} \frac{\rho v^2}{2} \quad (5)$$

Where  $f$  represents the frictional resistance coefficient;  $L$  represents the channel length;  $\rho$  represents density,  $v$  represents flow velocity; and  $De$  represents the equivalent diameter.

#### 2.1.1 Frictional pressure drop model

Many authors have conducted flow experiments on smooth rod bundles, investigated the frictional drag coefficient associated with

pressure drop, and formulated suitable frictional drag patterns for various working conditions and structures. The Blasius model (Hager, 2003) and the Rehme model (Rehme, 1972) are widely used to calculate the frictional pressure drop of smooth rod bundles. The correlations are:

Blasius model:

$$f = 0.316 Re^{-0.25} \quad \text{for } Re > 3000 \quad (6)$$

Rehme model:

$$\frac{1}{\sqrt{f_t}} = 2.035 \log Re \sqrt{f_t} - 0.989 \quad (7)$$

$$\frac{f}{f_t} = 1.045 + 0.71 (P/D - 1) \quad \text{for } 10^4 \leq Re \leq 10^5 \quad (8)$$

$$\frac{f}{f_t} = 1.036 + 0.054 (P/D - 1) \quad \text{for } Re \geq 10^5 \quad (9)$$

Where  $f_t$  is frictional resistance coefficient;  $f$  is the corrected frictional resistance coefficient.

Blasius model and Rehme model have been coupled into the sub-channel code.

### 2.1.2 Spacer loss coefficient model

The formula for calculating the grid-type spacers pressure drop is shown in Eq. (10),  $K$  is the spacer loss coefficient.

$$\Delta p = K \frac{\rho v^2}{2} \quad (10)$$

According to Rehme (Rehme and Trippe, 1980), the blockage of the flow cross section "e" of the spacer constitutes the main factor influencing the pressure loss, with the drag coefficient "K" being given by:

$$K = C_v e^2 \quad (11)$$

Where  $C_v$  is the modified loss coefficient;  $e$  is the relative closed cross-section ( $e = A_v/A_s$ , where  $A_v$  is the projected grid cross section and  $A_s$  the undisturbed flow section).

Cigarini later proposed empirical correlations (Cigarini and Donne, 1988) for  $e$  and  $C_v$  for spacer with rounded leading edges:

$$e = 0.6957 - 162.8 (p_s - d_s) \quad (12)$$

Where  $p_s$  is the pitch of the grid (m) and  $d_s$  is the rod diameter (m). The loss coefficient is given by:

$$C_v = 3.5 + \frac{73.14}{Re^{0.264}} + \frac{2.79 \times 10^{10}}{Re^{2.79}} \quad (13)$$

And finally:

$$K = \min[C_v e^2, 2] \quad (14)$$

## 2.2 Turbulent mixing models

Fuel assemblies featuring grid-type spacers are extensively utilized in various reactor types due to their straightforward design and low drag coefficient, leading to minimal pressure drop. Turbulent mixing pertains to the cross-flow mixing that arises from turbulent motion between distinct channels. The turbulent mixing coefficient ( $\beta$ ) is frequently employed to

TABLE 1 Turbulent mixing model.

Author	Relationship	Range of application
Wang (1983)	$\beta = 0.02968 Re^{-0.1}$	$46000 > Re > 90000$
Seale (1979)	$\beta = 0.009225 Re^{-0.1}$	$30000 > Re > 300000$
Petrunik (1968)	$\beta = 0.021 Re^{-0.1}$	$60000 > Re > 180000$
Rowe and Angle (1967)	$\beta = 0.063 Re^{-0.1}$	$42000 > Re > 126000$
Rogers and Tahir (1975)	$\beta = 0.007479 Re^{-0.1}$	$8100 > Re > 49500$

simulate cross-flow effects between different channels in sub-channel analysis. Numerous researchers have investigated the turbulent mixing coefficient for fuel assemblies with grid-type spacers. In this study, multiple turbulent mixing models are incorporated into a sub-channel code, as detailed in Table 1.

In the above models, the Petrunik model is applicable to the triangular fuel assembly with grid-type spacers, and the Reynolds number is close to the CiADS condition, so it is recommended for the subsequent thermal hydraulic calculation.

## 2.3 Heat transfer models

The heat transfer model is the most critical element for calculating fuel rod temperature in the sub-channel code. Therefore, choosing the appropriate model is pivotal for ensuring the accuracy of the sub-channel code. This study presents several widely-used heat transfer models in Table 2 and incorporates them into the sub-channel code. In 2014, J. Pacio et al. conducted an LBE heat transfer experiment and analyzed five different empirical formulas. Research indicates that the Mikityuk relationship exhibited the highest level of agreement with experimental results. The operational parameters of the CiADS triangular fuel assembly with grid-type spacers are:  $P/D = 1.38$ ,  $Pe = 200$ . Lastly, the sub-channel code couples various convection heat transfer models suited for different reactor types, thereby enhancing the program's versatility. The Mikityuk model is employed in the thermal hydraulic analysis of CiADS fuel assemblies with grid-type spacers.

## 3 Code validation

To investigate the thermal hydraulics of LBE eutectic in a reactor, a heat transfer experiment was conducted in 2016 at the KALLA Laboratory in Germany. The experiment involved a 19-rod fuel rod bundle equipped with grid-type spacers and used LBE as the coolant (Pacio et al., 2014). Over 80 different operating conditions were simulated, resulting in the collection of hundreds of experimental data points. These abundant experimental data offer valuable references for reactor design. In this study, the heat transfer experimental data from the 19-rod bundle with grid-type spacers, as conducted by Pacio, were selected as the validation benchmark. The computed data from the sub-channel analysis were compared with the experimental results to verify the accuracy of the calculations. The specific geometric parameters of the individual rods are detailed in Table 3, while the experimental conditions are outlined in Table 4. Temperature measurements were taken at distances of 532 and 855 mm

TABLE 2 Heat transfer model.

Authors	Formula	Range of applicability
Borishanskii (1969)	$Nu = 0.0174[1 - e^{-4(x-1)}](Pe - 200)^{0.9}$	$1.1 \leq P/D \leq 1.5, 0 \leq Pe \leq 2000$
Graber and Rieger (1972)	$Nu = 0.25 + 6.2x + (0.032x - 0.007)Pe^{0.8-0.024x}$	$1.2 \leq P/D \leq 2.0, 150 \leq Pe \leq 4000$
Ushakov (1978)	$Nu = 7.55x - 20x^{-13} + \frac{3.76}{90x^2}Pe^{0.56+0.19x}$	$P/D \leq 2.0, \leq Pe \leq 4000$
Mikityuk (2009)	$Nu = 0.047(1 - e^{-3.8(x-1)})(Pe^{0.77} + 250)$	$1.1 \leq P/D \leq 1.95, 30 \leq Pe \leq 5000$
Kazimi and Carelli (1976)	$Nu = 4.0 + 0.16x^5 + 0.33x^{3.8}(\frac{Pe}{100})^{0.86}$	$1.1 \leq P/D \leq 1.4, 10 \leq Pe \leq 5000$

TABLE 3 Terms rod parameters.

Parameters	Value (mm)
Rod outer diameter	8.2
Rod heated length	870
Rod total length	1272
Distance between rod centers	11.48
pitch-to-diameter ratio	1.4
Minimum distance to the channel	1.716

TABLE 4 Test matrix of experiments published by Pacio et al. (2014) made for different volumetric flow rate ( $V, m^3 h^{-1}$ ), thermal power ( $Q, kW$ ) and inlet Temperatures ( $T, ^\circ C$ ). Notes: —= no experiments. x =  $T_{in} = 200^\circ C$ . o =  $T_{in} = 300^\circ C$ .

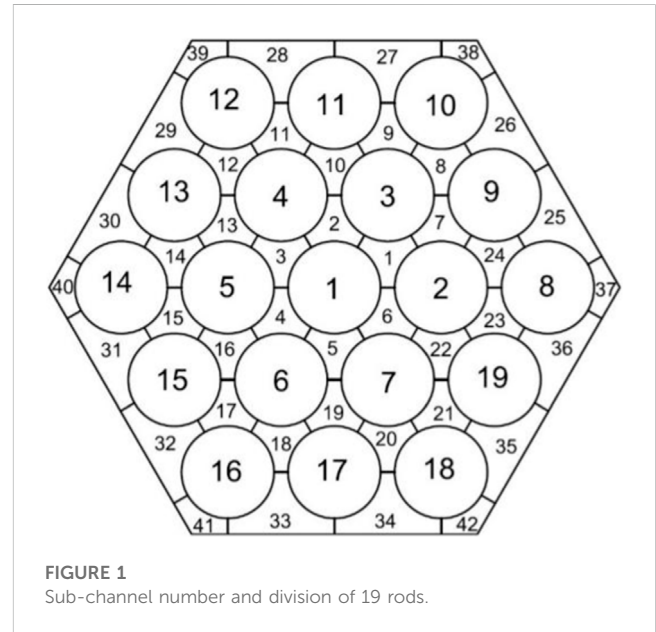
$V, m^3 h^{-1}$	Thermal power $Q, kW$							
	50	100	150	200	250	300	350	426
1.00	x	x	-	-	-	-	-	-
2.00	xo	xo	x	x	-	-	-	-
4.00	xo	xo	xo	xo	x	x	x	-
5.00	xo	xo	xo	xo	xo	x	x	x
6.00	xo	xo	xo	xo	xo	xo	x	x
8.00	xo	xo	xo	xo	xo	xo	xo	x
9.23	xo	xo	xo	xo	xo	xo	xo	xo
10.00	xo	xo	xo	xo	xo	xo	xo	xo

from the inlet of the heated section. This is illustrated in Figure 1, which provides a visualization of the sub-channel division.

Pacio et al. (2014) proposed a dimensionless temperature to describe the relative deviation between the temperature at the measurement location and the average temperature of the cross section. Equation 15 is used to describe this dimensionless temperature.

$$\theta = (T - T_{ave})\lambda / (q_w d_h) \tag{15}$$

Where  $T$  is measurement temperature (K);  $T_{ave}$  is average temperature (K);  $q_w$  is surface heat flux of the rod ( $W/m^2$ );  $d_h$  is equivalent diameter (m).



Figures 2A–D show the calculation results, which indicate good consistency between the sub-channel code calculations and experimental results. With increasing  $Pe$ , the turbulent mixing phenomenon becomes more apparent, and the difference between the wall temperature of R1 and the average temperature of the cross section gradually decreases, as does the difference between the temperature of sub-channel 33 and the average temperature of the cross section. The red and black lines represent the fitted results for the experimental and calculated data, respectively, offering a clearer visualization of their differences. The temperature distribution within each sub-channel also becomes more uniform. These observations are consistent with the anticipated outcomes, and the discrepancy between the non-dimensional cladding temperature and the non-dimensional coolant temperature, calculated using Eq. 15, remains within 0.03. As depicted in Eq. 15, changes in the dimensionless temperature are influenced by significant fluctuations in the measured or computed temperatures. With a temperature fluctuation of 10K, the impact on the dimensionless temperature reaches 0.05. This implies that there is a 10K error between the sub-channel code calculations and the experimental results, which could arise from uncertainties in the physical property relationships utilized in the code or inaccuracies in the experimental measurement equipment.



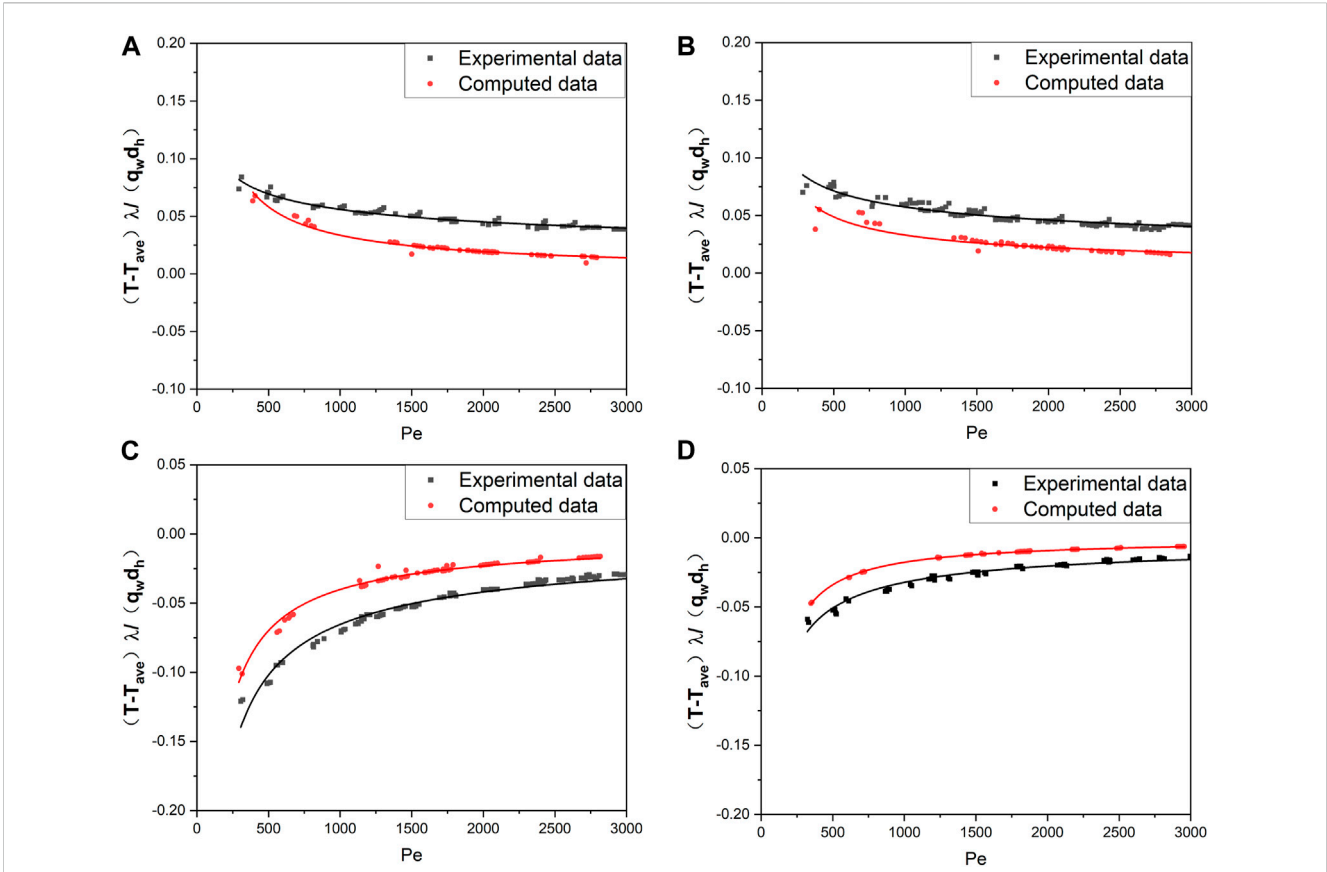


**FIGURE 2** (A) R1 non-dimensional wall temperature distribution at 532 mm, (B) R1 non-dimensional wall temperature distribution in 855 mm, (C) sub-channel 33 temperature distribution in 532 mm, (D) sub-channel 33 temperature distribution in 855 mm.

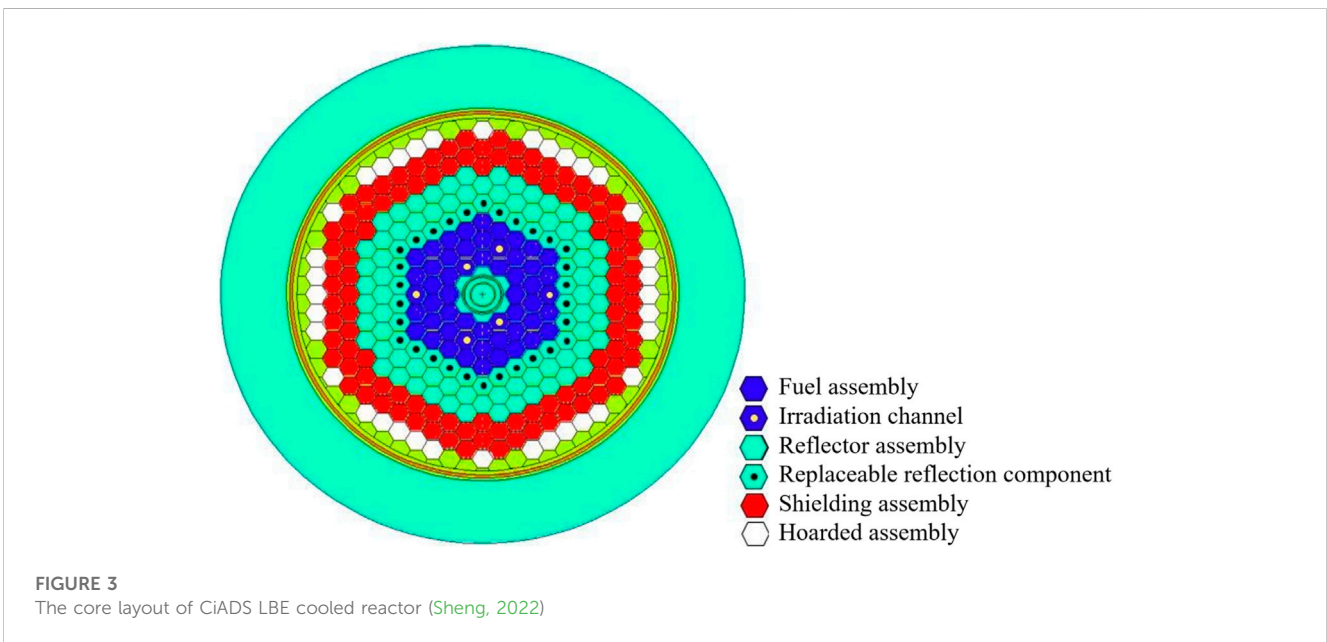


**FIGURE 3** The core layout of CiADS LBE cooled reactor (Sheng, 2022)

As mentioned earlier, the present sub-channel code possesses the capability to precisely compute coolant temperature and cladding outer surface temperature, enabling comprehensive

thermal hydraulic analysis of fuel assemblies featuring grid-type spacers. This capacity facilitates in-depth investigations into the characteristics of CiADS fuel assemblies.

TABLE 5 The design parameters of CiADS LBE cooled reactor core.

Parameters	Unit	Value
Total power (includes beam power)	MW	10
Thermal power	MW	9.76
Number of fuel assemblies		52
Heating section length	mm	1000
Inlet temperature	K	553
Outlet temperature	K	653
Upper limit of coolant temperature	K	729.6
Maximum fuel center temperature	K	807.44
Maximum surface temperature of cladding	K	733
Maximum burn-up	MWd/tU m/s	30,000
Maximum coolant velocity		2
Power distribution		Cosine distribution

TABLE 6 Structural dimensions of the fuel rods.

Parameters	Unit	Value
Fuel rod length	mm	1412
Fuel rod mass	kg	0.7995
Pellet material		UO <sub>2</sub>
Pellet diameter and height	mm	Φ8×10
Number of pellets		100
Cladding length	mm	1322
Outer diameter of cladding/thickness	mm	Φ9.7/0.7
Upper plug size	mm	Φ8.3 × 55
Lower plug size	mm	Φ8.3 × 55
Pressing spring size	mm	80
Insulating layer material	mm	YSZ (ZrO <sub>2</sub> -Y <sub>2</sub> O <sub>3</sub> )
Diameter and height of insulation layer	mm	Φ8×10
Air chamber height		200

## 4 Sub-channel thermal hydraulic analysis for CiADS fuel assembly

The main function of CiADS subcritical reactor core is coupling with accelerator and spallation target to generate strong fast neutron field and offer an experimental setting for nuclear waste transmutation. The CiADS LBE cooled reactor is designed to operate under subcritical conditions with power regulation by the accelerator beam. The core consists of 52 hexagonal fuel assemblies, a dummy assembly and associated test channels, with a circular hole in the middle for placing spallation target tubes. The core layout of CiADS LBE cooled reactor is shown in Figure 3, and the core design parameters are shown in Table 5.

### 4.1 CiADS fuel assembly structure

The fuel rod's overall structure consists of a lower plug, cladding tube, upper plug air chamber, fuel pellet, insulation layer, and compression spring. The lower end plug and upper end plug are connected to the cladding tube's upper and lower ends through ring welding, creating a sealed cavity. This cavity is arranged from top to bottom with an air chamber, multiple fuel pellets, a thermal insulation layer, and compression springs. The air chamber is designed to contain the gaseous fission products produced during fuel pellet operation, thereby preventing excessive internal pressure that could lead to cladding failure. The compression spring helps regulate the thermal expansion and radiation-induced swelling of the pellets. A specific amount of helium gas is filled within the fuel rods. This helium gas is situated between the fuel pellets and the inner cladding wall, enhancing heat conduction between them. Notches are present at the upper and lower ends to facilitate sliding connections with the upper and lower grids of the fuel assembly. Following established nuclear fuel production methods and related technology, fuel pellets enriched to 19.75% UO<sub>2</sub> ceramic composition were utilized. The fundamental structure of the fuel rod is illustrated in Figure 4, and pertinent dimensional parameters are provided in Table 6.

The fuel assembly features a hexagonal structure and is divided into four main parts: the bottom nozzle, weight-bearing area, fuel rod bundle area, and top nozzle. Externally, the fuel assembly is

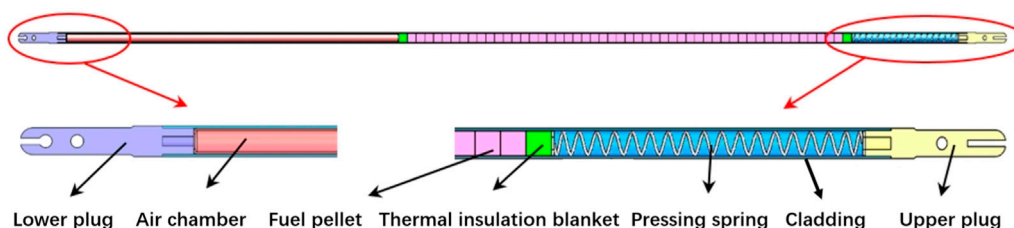


FIGURE 4 Structural composition of fuel rod (Sheng, 2022).

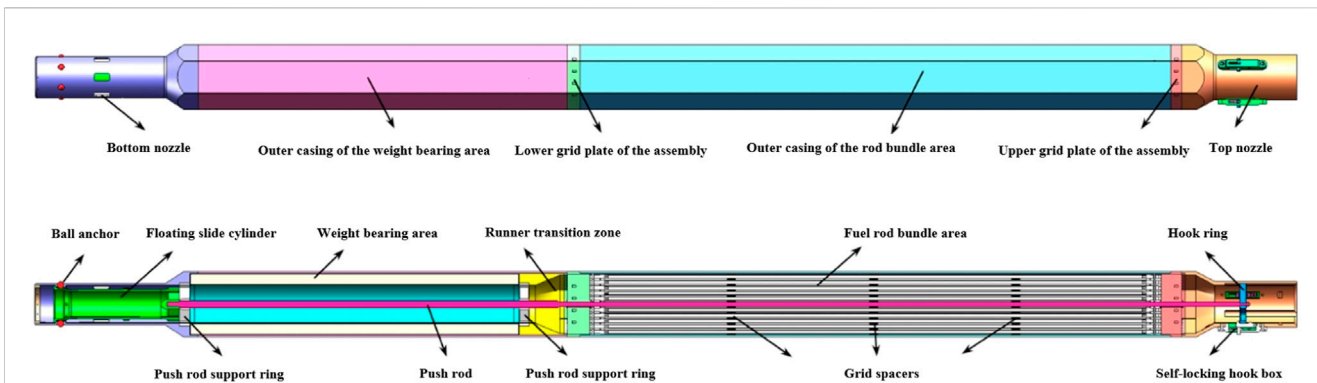


FIGURE 5 The structural composition of fuel assembly (Sheng, 2022).

TABLE 7 Structural dimensions of the fuel assemblies.

Parameters	Unit	Value
Assembly type	—	Closed hexagon assembly
Assembly length	mm	3077
Assembly weight	kg	243.7
Apothem	mm	137
Number of fuel rods		90
Pitch	mm	13.4
Grid-spacing ratio		1.381
Spacer grid-type		Cellular grid
Number of spacer grids		3
Lower tube seat height	mm	397
Lower seat diameter	mm	100
Height of counterweight area	mm	901
Counterweight mass	kg	117
Residual mass	kg	9.5
Rod bundle height	mm	1499
Upper tube seat height	mm	280
Upper seat diameter	mm	110
Length of push rod	mm	2641 (956 + 1685)
Push rod outer/inner diameter	mm	16/9.7
Number of self-locking hook box		3

composed of the bottom nozzle housing, the outer casing of the weight-bearing area, the lower grid plate of the assembly, the outer casing of the rod bundle area, the upper grid plate of the assembly, and the top nozzle housing. These components are sequentially welded and joined to form a closed structure that serves as the outer boundary of the fuel assembly. The internal structure primarily consists of three components. The first component is a push rod transmission mechanism, comprising a floating slide cylinder in the

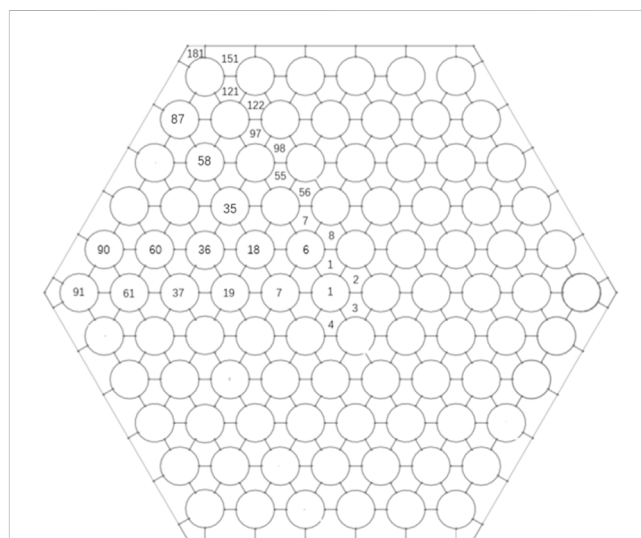
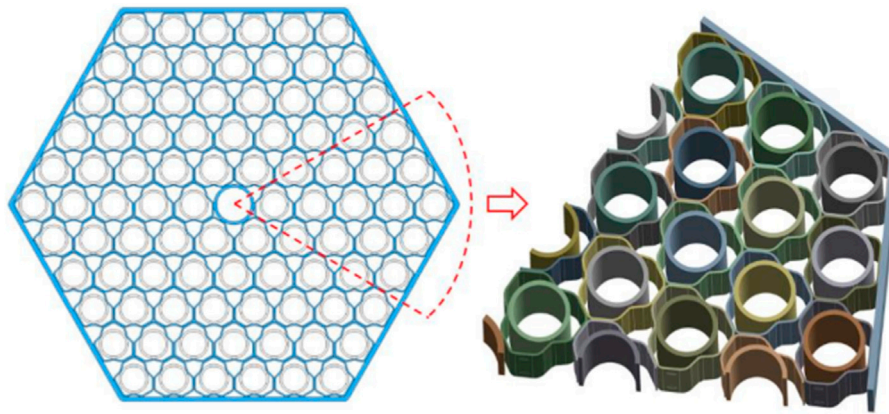


FIGURE 6 Sub-channel division and numbering of CiADS fuel assemblies.

lower tube seat, a push rod, and a hook ring in the upper tube seat. This mechanism facilitates the locking and unlocking function of the fuel assembly within the reactor core. The second component comprises metal tungsten blocks within the weight-bearing area, designed to counteract the buoyancy effect of LBE on the fuel assembly. The third component is the fuel rod bundle region, which serves as the core area of the fuel assembly. Its primary role is to generate nuclear heat and transfer it to the LBE cooling medium. Figure 5 illustrates the overall structure of the fuel assembly, while Table 7 presents the parameters of the fuel assembly.

The CiADS fuel assembly comprises 90 fuel rods and a control rod, with the fuel rods being held in place using grid-type spacers. The CiADS fuel assembly is divided into 186 sub-channels. The specific division and numbering of these sub-channels are illustrated in Figure 6, while the structural design of the CiADS fuel assembly's grid-type spacers is shown in Figure 7. The grid-type spacers of the fuel assembly are constructed from 72 intermediate grid elements, 18 edge grid elements, and edge strips, all of which are welded together. Each grid element is designed to accommodate fuel rods.





**FIGURE 7**  
Structural design of CiADS fuel assembly grid-type spacers (Sheng, 2022).

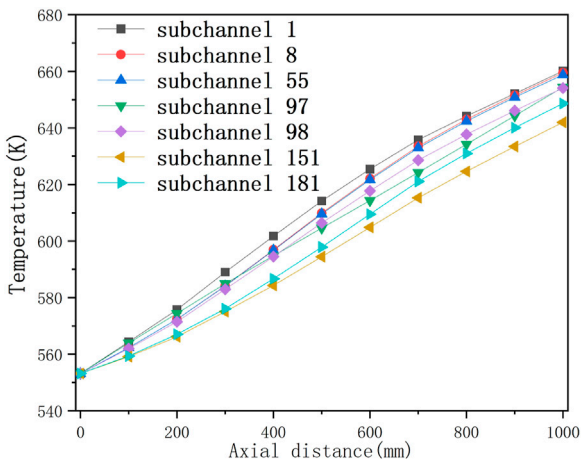


**FIGURE 8**  
Calculated axial temperature distribution of the coolant in 7 different sub-channels in CiADS fuel assembly.

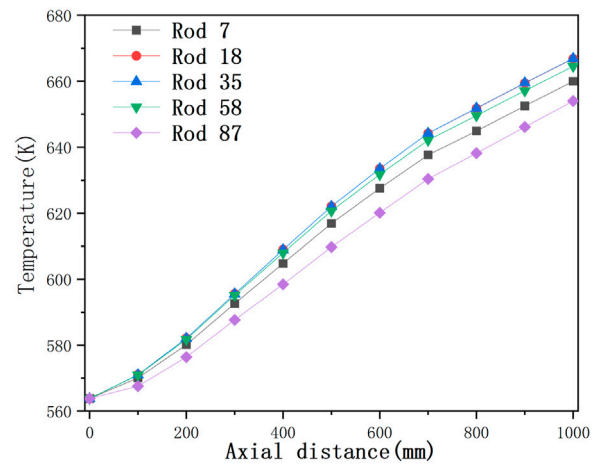


**FIGURE 9**  
Temperature distribution of cladding at 5 different rods in CiADS fuel assembly.

To secure the CiADS fuel assembly, three positioning grids are strategically placed at 1/4, 1/2, and 3/4 positions along the length of the fuel assembly.

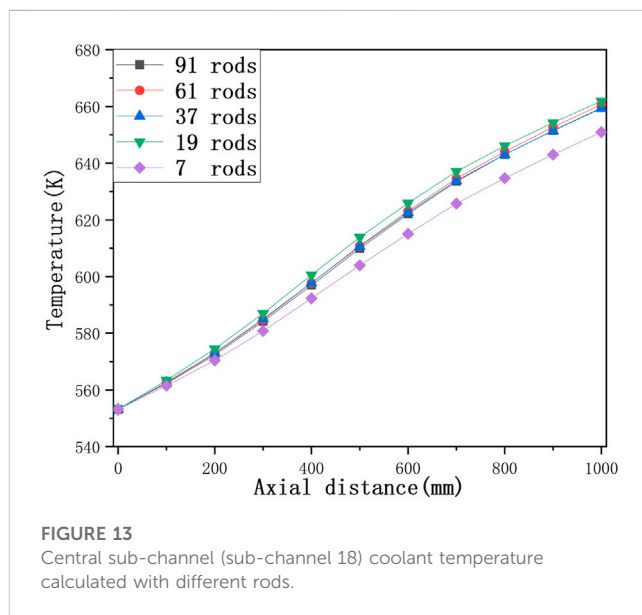
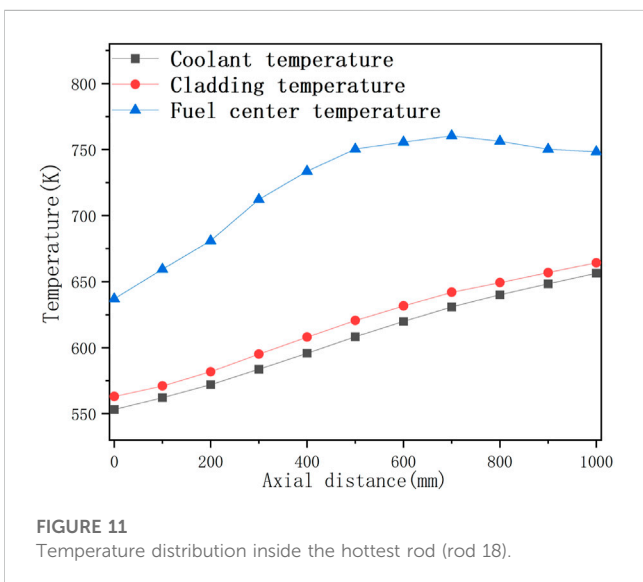
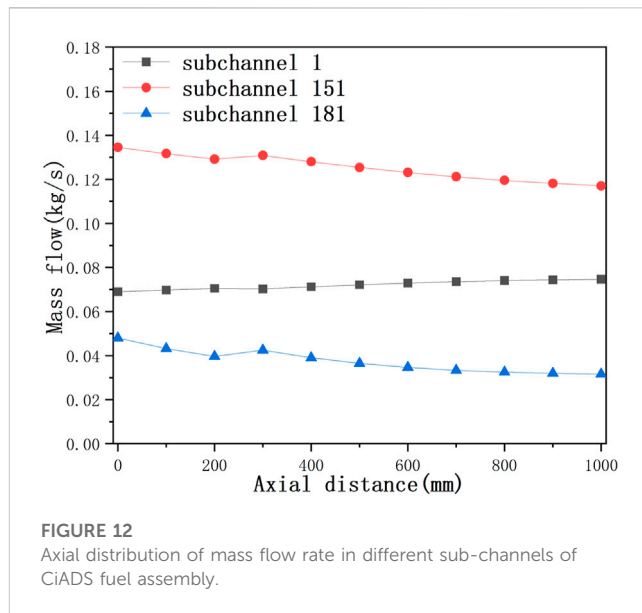
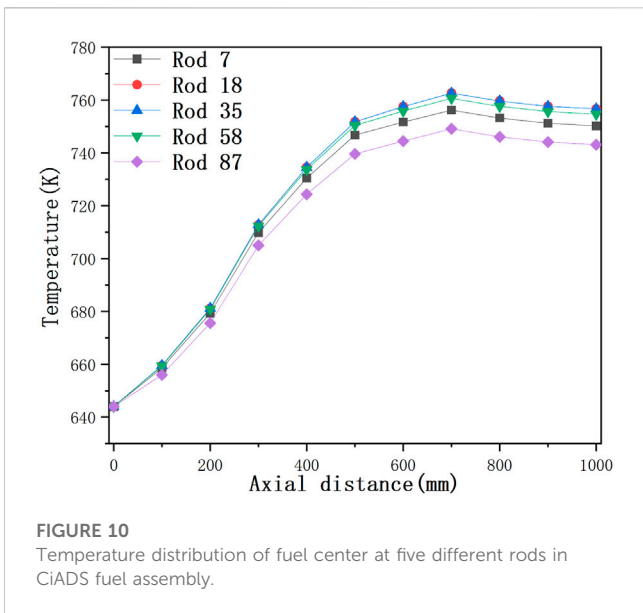
### 4.2 Coolant temperature distribution

To emphasize the contrast in coolant temperature between the inner and outer channels, this study chose seven sub-channel temperatures from various positions, ranging from the innermost to the outermost. As shown in Figure 8, in external channels, the corner channel exhibits a higher temperature than the side channel. This can be attributed to the side channel having a flow area three times larger than the corner channel, yet its overall heat transfer is just 1.5 times that of the corner. Furthermore, the fluid’s mass flow rate is greater in the side channel than in the corner channel. The calculation results indicate that the maximum coolant temperature occurs in sub-channel 8, reaching 660.16 K, which is lower than the

maximum design temperature of 1823.15 K for the CiADS core coolant.

### 4.3 Fuel rods temperature distribution

Figure 9 illustrates the distribution of cladding temperatures for different rods. The highest cladding temperature was recorded in rod 18, reaching 666.92 K, which remains below the CiADS design limit of 823.15 K. The temperature distribution of the cladding and the fuel center mirrors that of the coolant, with the fuel rods situated closer to the center exhibiting higher temperatures. Figure 10 displays the maximum fuel center temperature as 756.65 K, meeting the CiADS design requirement of 1523.15 K. The elevated cladding and fuel temperatures observed in rod 18, in comparison to other rods, can be attributed to its central position within the fuel assembly and the absence of heat sources from control rods. Positioned

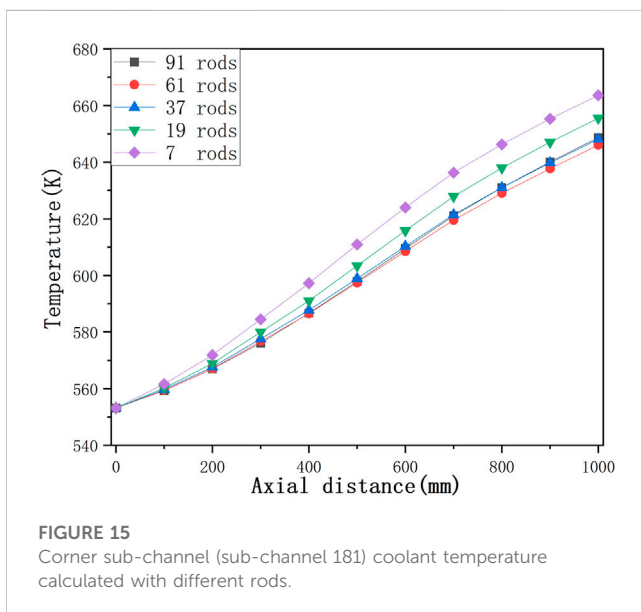
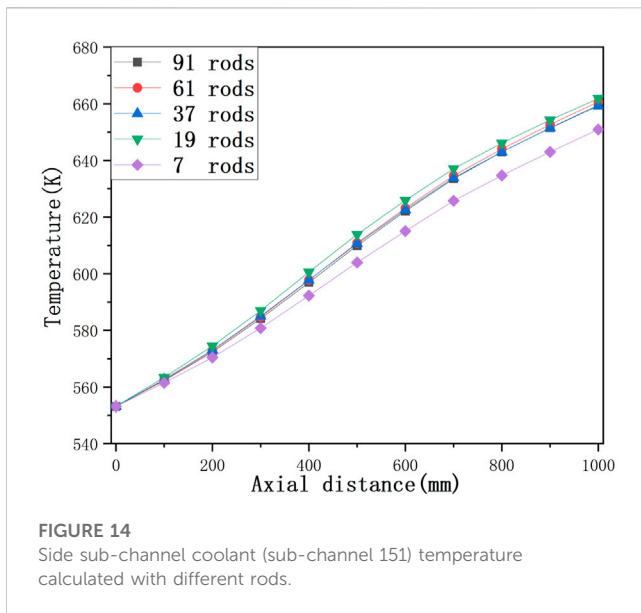


near the second ring of control rods, rod 18 experiences higher coolant temperatures in the surrounding sub-channels than other rod bundles. Consequently, this leads to relatively higher cladding and fuel temperatures calculated based on the coolant temperature.

Figure 11 presents the temperature profile of the hottest fuel rod among the 90 heated rods, depicting the coolant temperature, cladding temperature, and fuel center temperature. Owing to the cosine distribution of heat sources within the fuel rod, the thermal power density is heightened in the central section of the rod. Consequently, the calculated fuel rod temperatures, established on the thermal power density and coolant temperature, peak in the rear section of the central region before gradually declining.

### 4.4 Mass flow rate distribution

The mass flow rates of the inner channel, side channel, and corner channel are depicted in Figure 12. The results indicate a gradual increase in the mass flow rate of the inner channel, while the mass flow rates of the side channel and corner channel gradually decrease. As the coolant flows, the mass flow rate of the coolant within the grid-type spacers fuel assembly exhibits a trend of being higher in the central sub-channels and lower in the corner channels. This observation corroborates the conclusion that the temperature of the inner channel is higher than that of the side channel and corner sub-channel, as shown in Figure 8.



#### 4.5 Different number of rods analysis

In the context of the CFD method, smaller-sized rod bundle simulations are often employed instead of larger-sized ones, while maintaining calculation accuracy. Although certain calculation errors might arise due to the omission of certain conditions, substantial computational resources can be conserved. This approach is also adopted in sub-channel codes, wherein the rod bundle size is reduced for calculation while keeping the boundary conditions unchanged. In this study, calculations were performed for rod bundles consisting of 91 rods, 61 rods, 37 rods, 19 rods, and 7 rods, and the corresponding results are presented in Figures 13–15. The outcomes of the 61-rods and 37-rods cases closely resemble the simulation results obtained from calculations involving the

full assembly of rods. To optimize computational efficiency, the simulation outcomes from the 37-rods case are recommended for use as a substitute for the simulation results of the full assembly. This approach enables significant computational resource savings without significantly compromising the reliability of the results.

## 5 Conclusion

Building upon the sub-channel code developed by Liu et al. for thermal hydraulic analysis of LBE wound wire fuel assemblies, this study conducted a secondary development. A thermal hydraulic analysis code was developed specifically for fuel assemblies of LBE cooled fast reactors with grid-type spacers. A comparison was made between the results of the 19-rod flow heat transfer experiment carried out by Pacio and the calculations of coolant temperature to verify the code's accuracy. Furthermore, an analysis was performed on the CiADS 91-rod fuel assembly using the sub-channel analysis code, based on design parameters. The analysis investigated the impact of coolant temperature, fuel rod temperature, coolant mass flow rate, and rod bundle arrangement. The findings can be summarized as follows:

Different models were evaluated for their applicability, and the Rehme, Petrunik, and Mikityuk models were recommended for calculating friction pressure drop, turbulent mixing, and convective heat transfer in CiADS sub-channel analysis.

The results from the code calculations closely aligned with the experimental data. As the Péclet number ( $Pe$ ) increased, the temperatures of various sub-channels tended to approach the average temperature.

The code's calculations indicated that the maximum coolant temperature occurred in sub-channel 8, while the maximum fuel rod temperature was in rod 18. Under steady operating conditions, the maximum fuel center temperature reached 756.65 K, and the maximum cladding temperature was 666.92 K.

By analyzing different rod numbers, it was determined that 37 rods were recommended as the minimum rod bundle configuration for simulating the full-scale fuel assembly.

## Data availability statement

The raw data supporting the conclusions of this article will be made available by the authors, without undue reservation.

## Author contributions

Q-JC: Conceptualization, Data curation, Investigation, Methodology, Software, Validation, Writing–original draft, Writing–review and editing. JQ: Conceptualization, Investigation, Software, Writing–original draft, Writing–review and editing. J-BZ: Conceptualization, Investigation, Writing–original draft, Writing–review and editing. Y-FG: Conceptualization, Investigation, Methodology, Software, Writing–original draft, Writing–review and editing. X-KS:

Conceptualization, Formal Analysis, Funding acquisition, Project administration, Software, Writing—original draft, Writing—review and editing. LG: Conceptualization, Funding acquisition, Project administration, Software, Writing—original draft, Writing—review and editing. J-TL: Investigation, Software, Writing—original draft, Writing—review and editing.

## Funding

The author(s) declare financial support was received for the research, authorship, and/or publication of this article. This work is finally supported by the China Postdoctoral Science Foundation (2023M731458), the Gansu Natural Science Foundation (23JRR1099), and the China Natural Science Foundation (12122512).

## References

- Abderrahim, H. A., Baeten, P., De Bruyn, D., and Fernandez, R. (2012). MYRRHA—A multi-purpose fast spectrum research reactor. *Energy Convers. Manag.* 63, 4–10. doi:10.1016/j.enconman.2012.02.025
- Abram, T., and Ion, S. J. E. P. (2008). Generation-IV nuclear power: A review of the state of the science. *A Rev. state Sci.* 36, 4323–4330. doi:10.1016/j.enpol.2008.09.059
- Borishanskii, V. M., Gotovskii, M. A., and Firsova, E. V. (1969). Heat transfer to liquid metals in longitudinally wetted bundles of rods. *Sov. At. Energy* 27 (6), 1347–1350. doi:10.1007/bf01118660
- Chen, , et al. (2012). Sub-channel model of Analysis cold fast ATHAS-LMR for LMFR. *Atomic Energy Sci. Technol.* 46 (6), 695–700. doi:10.1115/ICONE26-81600
- Cigarini, M., and Donne, M. D. (1988). Thermohydraulic optimization of homogeneous and heterogeneous advanced pressurized water reactors. *Nucl. Technol.* 80 (1), 107–132. doi:10.13182/nt88-a35553
- Di Piazza, I., Angelucci, M., Marinari, R., Tarantino, M., and Forgione, N. (2016). Heat transfer on HLM cooled wire-spaced fuel pin bundle simulator in the NACIE-UP facility. *Nucl. Eng. Des.* 300, 256–267. doi:10.1016/j.nucengdes.2016.02.008
- George, T., Basehore, K., Wheeler, C., et al. (1980). *COBRA-WC: A version of COBRA for single-phase multiassembly thermal hydraulic transient analysis*. Richland, WA, USA: Battelle Pacific Northwest Laboratories. Available at: [http://refhub.elsevier.com/S0149-1970\(18\)30250-6/sref11](http://refhub.elsevier.com/S0149-1970(18)30250-6/sref11).
- Gräber, H., and Rieger, M. (1972). Experimentelle Untersuchung des Wärmeübergangs an Flüssigmetalle (NaK) in parallel durchströmten Rohrbündeln bei konstanter und exponentieller Wärmeflussdichteverteilung. *Atomkernenerg. (ATKE) Bd* 19, 23–40.
- Gu, L., and Su, X. K. (2021). Latest research progress for LBE coolant reactor of China initiative accelerator driven system project. *Front. Energy.* 15 (4), 810–831. doi:10.1007/s11708-021-0760-1
- Hager, W. H. (2003). Blasius: A life in research and education. *Exp. Fluids* 34 (5), 566–571. doi:10.1007/s00348-002-0582-9
- Kazimi, M. S., and Carelli, M. D. (1976). *Clinch River breeder reactor plant. Heat transfer correlation for analysis of CRBRP assemblies*. Madison, PA United States: Westinghouse Electric Corp.
- Kim, W. S., Kim, Y. G., and Kim, Y. J. (2002). A sub-channel analysis code MATRA-LMR for wire wrapped LMR subassembly. *Ann. Nucl. Energy* 29 (3), 303–321. doi:10.1016/s0306-4549(01)00041-x
- Li, J. Y., He, Z. Y., Gu, L., Zhang, Y. P., Xu, H. S., Yao, C. F., et al. (2021). The temperature control of the dense granular spallation target in China initiative accelerator driven system based on quantum evolutionary algorithm. *Prog. Nucl. Energy* 131, 103587. doi:10.1016/j.pnucene.2020.103587
- Li, S., Cao, L., Khan, M. S., and Chen, H. (2017). Development of a sub-channel thermal hydraulic analysis code and its application to lead cooled fast reactor. *Appl. Therm. Eng.* 117, 443–451. doi:10.1016/j.applthermaleng.2017.02.044
- Liu, J. T., Peng, T. J., Wang, G., Su, X. K., Tao, Y. J., Fan, D. J., et al. (2022). Sub-channel analysis of lead–bismuth fast reactor fuel assembly with wire spacers for China

## Conflict of interest

Author J-TL were employed by China Nuclear Power Engineering Co LTD.

The remaining authors declare that the research was conducted in the absence of any commercial or financial relationships that could be construed as a potential conflict of interest.

## Publisher's note

All claims expressed in this article are solely those of the authors and do not necessarily represent those of their affiliated organizations, or those of the publisher, the editors and the reviewers. Any product that may be evaluated in this article, or claim that may be made by its manufacturer, is not guaranteed or endorsed by the publisher.

initiative accelerator driven system. *Ann. Nucl. Energy* 170, 108965. doi:10.1016/j.anucene.2021.108965

Lodi, F., Grasso, G., Mattioli, D., and Sumini, M. (2016a). ANTEO+: A sub-channel code for thermal-hydraulic analysis of liquid metal cooled systems. *Nucl. Eng. Des.* 301, 128–152. doi:10.1016/j.nucengdes.2016.03.001

Lodi, F., Grasso, G., Mattioli, D., and Sumini, M. (2016b). ANTEO+: A sub-channel code for thermal-hydraulic analysis of liquid metal cooled systems. *Nucl. Eng. Des.* 301, 128–152. doi:10.1016/j.nucengdes.2016.03.001

Lyu, K., Chen, L., Yue, C., Gao, S., Zhou, T., and Huang, Q. (2016). Preliminary thermal-hydraulic sub-channel analysis of 61 wire-wrapped bundle cooled by lead bismuth eutectic. *Ann. Nucl. Energy* 92, 243–250. doi:10.1016/j.anucene.2016.01.034

Mikityuk, K. (2009). Heat transfer to liquid metal: review of data and correlations for tube bundles. *Nucl. Eng. Des.* 239 (4), 680–687. doi:10.1016/j.nucengdes.2008.12.014

Pacio, J., Daubner, M., Fellmoser, F., Litfin, K., Marocco, L., Stieglitz, R., et al. (2014). Heavy-liquid metal heat transfer experiment in a 19-rod bundle with grid spacers. *Nucl. Eng. Des.* 273, 33–46. doi:10.1016/j.nucengdes.2014.02.020

Peng, T. J., Gu, L., W, D. W., et al. (2017). Conceptual design of subcritical reactor for China initiative accelerator driven system. *Atomic Energy Sci. Technol.* 51 (12), 2235. doi:10.7538/yzk.2017.51.12.2235

Petrunik, K. J. (1968). *Turbulent mixing measurements for single phase air, single phase water, and two-phase air-water flows in adjacent rectangular sub-channels*. Windsor, ON, Canada: University of Windsor.

Rehme, K., and Trippe, G. (1980). Pressure drop and velocity distribution in rod bundles with spacer grids. *Nucl. Eng. Des.* 62 (1-3), 349–359. doi:10.1016/0029-5493(80)90038-2

Rehme, K. (1973). Pressure drop correlations for fuel element spacers. *Nucl. Technol.* 17 (1), 15–23. doi:10.13182/nt73-a31250

Rogers, J. T., and Tahir, A. E. E. (1975). Turbulent interchange mixing in rod bundles and the role of secondary flows. *Pap. Am. Soc. Mech. Eng.* 75.

Rowe, D. S., and Angle, C. W. (1967). *Crossflow mixing between parallel flow channels during boiling. Part ii. Measurement of flow and enthalpy in two parallel channels*. Richland, WA, USA: Pacific Northwest Lab. Available at: [http://refhub.elsevier.com/S0029-5493\(20\)30020-0/h0100](http://refhub.elsevier.com/S0029-5493(20)30020-0/h0100).

Rowe, D. S. (1970). *COBRA-II: A digital computer program for thermal-hydraulic sub-channel analysis of rod bundle nuclear fuel elements*. Richland, WA, USA: Battelle Pacific Northwest Laboratories. Available at: [https://inis.iaea.org/collection/NCLCollectionStore/\\_Public/01/001/1001764.pdf](https://inis.iaea.org/collection/NCLCollectionStore/_Public/01/001/1001764.pdf).

Schroer, C., Wedemeyer, O., Skrypnik, A., Novotny, J., and Konys, J. (2012). Corrosion kinetics of steel T91 in flowing oxygen-containing lead–bismuth eutectic at 450 °C. *J. Nucl. Mater.* 431 (1-3), 105–112. doi:10.1016/j.jnucmat.2011.11.014

Seale, W. J. (1979). Turbulent diffusion of heat between connected flow passages Part 1: outline of problem and experimental investigation. *Nucl. Eng. Des.* 54 (2), 183–195. doi:10.1016/0029-5493(79)90166-3

- Sheng, X. (2022). *Research on structure and mechanical properties of fuel assembly for CiADS lead bismuth fast reactor*. Guangdong, China: Institute of Modern Physics, Chinese Academy of Sciences. Available at: [https://kns.cnki.net/kcms2/article/abstract?v=3uoqIhG8C447WN1SO36whLpCgh0R0Z-i16\\_wNaYct1rCckkTLVqOrEKIRUCgs4uTvPKdTTxjIGezYHmuj\\_9ee6dLN2orMlJs&uniplatform=NZKPT](https://kns.cnki.net/kcms2/article/abstract?v=3uoqIhG8C447WN1SO36whLpCgh0R0Z-i16_wNaYct1rCckkTLVqOrEKIRUCgs4uTvPKdTTxjIGezYHmuj_9ee6dLN2orMlJs&uniplatform=NZKPT).
- Ushakov, P. A., Zhukov, A. V., and Matyukhin, N. M. (1978). Heat transfer to liquid metals in regular arrays of fuel elements. *High. Temp. USSR Engl. Transl. U. S.* 15 (5).
- Wang, C., Wu, D., Gui, M., Cai, R., Zhu, D., Zhang, D., et al. (2021). Flow blockage analysis for fuel assembly in a lead-based fast reactor. *Nucl. Eng. Technol.* 53 (10), 3217–3228. doi:10.1016/j.net.2021.05.007
- Wang, J., Tian, W., Tian, Y., Su, G., and Qiu, S. (2013a). A sub-channel analysis code for advanced lead bismuth fast reactor. *Prog. Nucl. Energy* 63, 34–48. doi:10.1016/j.pnucene.2012.09.010
- Wang, J., Tian, W. X., Tian, Y. H., Su, G., and Qiu, S. (2013b). A sub-channel analysis code for advanced lead bismuth fast reactor. *Prog. Nucl. Energy* 63, 34–48. doi:10.1016/j.pnucene.2012.09.010
- Wang, Z., Jia, D., and Yu, Z. (1983). Experiment investigation on the turbulent mixing between sub-channels for single-phase flow in a simulated bundle. *Chin. J. Nucl. Sci. Eng.* 3 (2), 106–114.
- Wu, D., Wang, C., Gui, M., Lan, Z., Lu, Q., Zhang, D., et al. (2021). Improvement and validation of a sub-channel analysis code for a lead-cooled reactor with wire spacers. *Int. J. Energy Res.* 45 (8), 12029–12046. doi:10.1002/er.6015
- Yu, R., Gu, L., Sheng, X., Li, J., Zhu, Y., Zhang, L., et al. (2021). Review of fuel assembly design in lead-based fast reactors and research progress in fuel assembly of China initiative accelerator driven system. *Int. J. Energy Res.* 45 (8), 11552–11563. doi:10.1002/er.6569
- Zhan, W. L., and Xu, H. S. (2012). Advanced fission energy program - ADS transmutation system. *Bull. Chin. Acad. Sci.* 27, 375–381.